

## Effect of Milling Energy and Process Ordering on the Morphologies and Optical Properties of ZnO Nanoparticles Obtained Through a Mechanochemical Technique

Zahra Makhdoomi Kakhaki,\* Amirali Youzbashi and Nima Naderi

Materials and Energy Research Center, P.O. Box 14155-4777, Tehran-Iran

\*Corresponding author: zahramakhdoomi@yahoo.com

**Abstract:** Zinc oxide (ZnO) nanoparticles were synthesised by a mechanochemical method using  $\text{ZnCl}_2$  and  $\text{Na}_2\text{CO}_3$  as precursors and NaCl as a diluent. The effects of the milling energy, influenced by factors such as the milling time and ball-to-powder mass ratio, and the ordering of the synthetic stages on the structure, morphology and optical properties of the synthesised nanoparticles were characterised by X-ray diffraction, scanning electron microscopy, and transmission electron microscopy, as well as by UV-visible and photoluminescence spectroscopies. The results indicated the direct formation of ZnO nanoparticles after 10 hours of milling, without the need for heat treatment, as a result of the high-energy milling process. The crystallite sizes of the nanoparticles increased with higher milling times and ball-to powder mass ratios due to cold welding. ZnO nanoparticles with crystallite sizes in the range of 16 nm–19 nm were produced through optimisation of the order of synthetic stages and milling energy. Different morphologies were obtained in different samples due to the effects of changing the order of the synthetic steps. The optical band gap of the synthesised ZnO nanoparticles was lower than in bulk samples because of the presence of defects.

**Keywords:** ZnO nanoparticles, one-step mechanochemical method, milling energy, band gap, morphology

### 1. INTRODUCTION

Zinc oxide (ZnO) has a wide, direct band gap (3.37 eV) with a large exciton binding energy (60 meV) and stable wurtzite structure with lattice spacings of  $a = 0.325$  nm and  $c = 0.521$  nm. It is commonly used in many important applications, such as in solar cells,<sup>1</sup> gas sensors,<sup>2</sup> electronics,<sup>3</sup> pigments<sup>4</sup> and photocatalysts.<sup>5</sup> Both particle size and morphology have a strong influence on the properties and potential applications of ZnO nanoparticles.<sup>6–8</sup> Different methods are currently utilised for the preparation of ZnO nanostructures, including chemical (co-precipitation<sup>9</sup> and sol-gel<sup>10</sup>), physical (physical vapour deposition<sup>11</sup>), and mechanical (mechanical milling<sup>12–14</sup> and mechanochemical<sup>15</sup>) methods. Mechanochemical synthesis is a simple, economical and convenient method, which is suitable for large-scale production

of nanoparticles. Mechanochemical processing may be described as the repeated welding, deformation and fracture of a mixture of reactants. Chemical reactions occur at the interfaces of nano-grains that are continuously re-generated during milling.<sup>16</sup> The most important requirement of this technique is the formation of separated nanoparticles embedded in a salt matrix, which in turn leads to agglomerate-free nanopowders.<sup>17</sup> The removal of the salt matrix is generally carried out through simple washing.

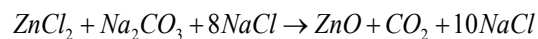
Mechanochemical syntheses of ZnO nanoparticles have been reported through different methods using various precursors. In the first such synthesis, Tsuzuki and McCormick<sup>18</sup> carried out a solid-state displacement reaction between  $ZnCl_2$  and  $Na_2CO_3$ , forming  $ZnCO_3$  in a NaCl matrix by a mechanochemical technique. Subsequent heat treatment was used in order to decompose  $ZnCO_3$  into ZnO nanoparticles. This approach was further developed by other researchers.<sup>19,20</sup> Dhara and Giri synthesised ZnO nanoparticles by milling a mixture of zinc acetate, N-cetyl-N, N, N-trimethyl ammonium bromide, a cationic surfactant and sodium hydroxide, followed by calcination of the milled powder mixture.<sup>21</sup> Jun et al. produced ZnO nanoparticles in a one-step mechanochemical reaction without heat treatment using zinc sulfate and sodium hydroxide or potassium hydroxide as reactants and sodium chloride or potassium chloride as diluents.<sup>22</sup>

To the best of our knowledge, the effects of milling time and ball-to-powder mass ratio on the one-step mechanochemical reaction of  $ZnCl_2$  and  $Na_2CO_3$  and the effects of the ordering of the synthetic stages on the morphology of ZnO nanoparticles presented in the present work have not yet been reported.

## 2. EXPERIMENTAL DETAILS

### 2.1 Materials

The materials used in this research were anhydrous  $ZnCl_2$ , anhydrous  $Na_2CO_3$ , and NaCl purchased from Merck. The NaCl was used as a diluent. The reaction between the starting materials proceeds as follows:



### 2.2 Synthetic Procedure

The starting materials were mixed in a 300 ml stainless steel vessel containing three stainless steel balls with 20 mm diameters, nine balls with 15

mm diameters, and 17 balls with 10 mm diameters. The milling rate was set to 300 rpm. Milling was carried out in a high-energy planetary ball mill (model retsch pm400) over a range of milling times between eight and 14 hours and with ball-to-powder mass ratios of 15:1 and 20:1.

After milling, three groups of samples were obtained. The first group was milled and washed with doubly deionised (DDI) water, subjected to centrifugal separation to remove NaCl, and heated to 400°C for approximately two hours. The second group was milled and washed, and the third group was milled, heated and then washed.

The samples obtained through this mechanochemical synthesis were denoted as Sample A and Sample B for the first group, Sample C and Sample D for the second group and Sample E for the third group. The conditions of the mechanochemical treatment for various samples are listed in Table 1.

Table 1: The conditions of mechanochemical process for different samples.

Sample code	A	B	C	D	E
Milling time (hour)	8	10	12	14	8
Ball to powder mass ratio	15:1	20:1	15:1	20:1	15:1
Stages ordering of synthesis	Milling, washing and heating	Milling, washing and heating	Milling and washing	Milling and washing	Milling, heating and washing

### 2.3 Characterisation of ZnO Nanoparticles

The samples were characterised by X-ray diffraction (XRD) on a Siemens D500 diffractometer using Cu K $\alpha$  radiation, scanning electron microscopy (SEM) using a Hitachi S-410 vacc 25 kv microscope, transmission electron microscopy (TEM) using a Phillips CM-200 microscope, UV-vis spectroscopy on a PerkinElmer spectrometer (LambdaIs USA), and photoluminescence (PL) analysis on a Perkin Elmer – LS-5 spectrometer with a starting wavelength of 320 nm.

### 3. RESULTS AND DISCUSSION

#### 3.1 The Morphology and Structure of ZnO Nanoparticles

Figures (1–3) shows the XRD patterns of samples prepared with different ordering of their synthetic stages. The XRD patterns of all the samples after the milling process consisted of ZnO and NaCl peaks. However, no peaks indicative of  $\text{ZnCl}_2$  or  $\text{Na}_2\text{CO}_3$  phases were observed. In contrast to previous results<sup>17</sup> wherein the  $\text{ZnCO}_3$  and NaCl phases were reported as the major products after milling, we found that the ZnO and NaCl phases were the major post-milling products. This is due to the application of a milling energy sufficient for the decomposition of zinc carbonate and production of ZnO during the milling process. The dominant peak in the post-milling XRD patterns of samples a-e was related to NaCl. In these samples, the intensity of the ZnO peak was relatively low.

The XRD patterns of samples c and d recorded after the milling-washing stages are presented in Figure 2. All of the diffraction peaks corresponded to a hexagonal ZnO phase (JCPDS card no. 36-1451), indicating the complete absence of impurity phases and the direct synthesis of ZnO nanoparticles without heat treatment. According to Figure 1, both ZnO and hydroxyzincite ( $\text{Zn}_5(\text{OH})_6(\text{CO}_3)_2$ ) phases were observed after the milling-washing process due to the application of insufficient milling energy to induce the direct synthesis of ZnO nanoparticles. Thus, Samples A and B were heated at 400°C for two hours to obtain ZnO nanoparticles. The XRD pattern of Sample E after the milling-heating stage consisted of intense peaks related to a NaCl phase and a less intense peak related to the ZnO phase. As shown in Figure 3, ZnO nanoparticles were obtained after the milling-heating-washing process. The crystallite sizes of samples a-e were calculated after the final synthetic steps from the full width at half maximum (FWHM) of the relevant XRD peaks using the Debye-Scherrer equation. The crystallite sizes of Samples A–E were 16.6, 17.5, 16.1, 18.9 and 16.5 nm, respectively. Despite the fact that the ordering of the synthetic steps used for Samples A and E were different, their crystallite sizes were nearly the same. The crystallite size for Sample C was smaller than for Sample D because of cold welding during the high-energy milling process, which caused the agglomeration of particles in Sample D. The crystallite size for Sample C was smaller than for Samples A, B and E due to the lack of heat treatment. The crystallite size for sample d was greater than for other samples because of cold welding and agglomeration. Increasing the milling energy caused the capacity of particles to undergo further plastic deformation to decrease. Because welding was the dominant mechanism in the mechanochemical process, the particles agglomerated.

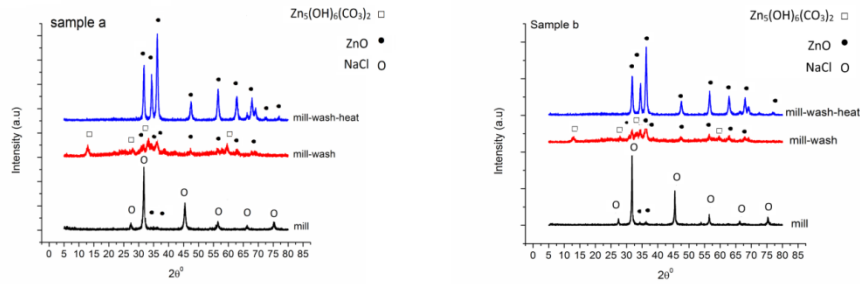


Figure 1: The XRD patterns of Samples A and B.

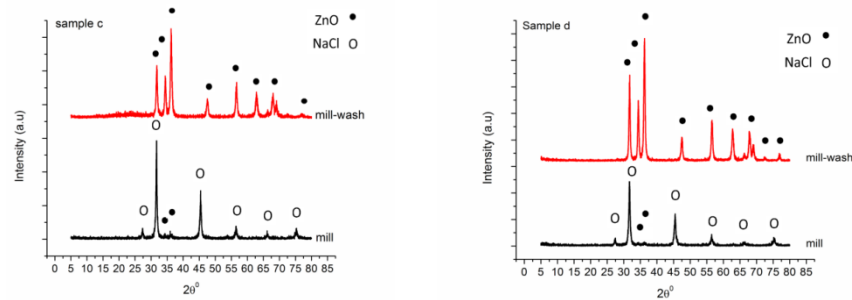


Figure 2: The XRD patterns of Samples C and D.

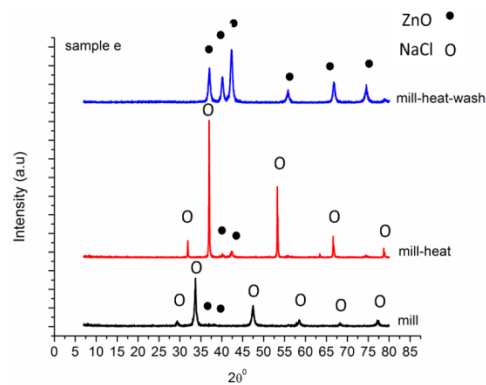


Figure 3: The XRD patterns of Sample E.

Figure 4 presents the SEM micrographs of ZnO nanoparticles in Samples A, D and E and a TEM micrograph of Sample D. Based on Figure 4, the morphologies of Samples A and D after the final process (milling, washing, and heating) were spherical, while Sample E had a flake-shape morphology. This morphology could be due to the embedding of diluent phase (NaCl) in the ZnO nanoparticles during the heat treatment stage and the inhibition of the formation of spherical nanoparticles. The thickness of the flakes was  $\sim 30$  nm. Samples A

and D consisted of agglomerated spherical particles. The TEM micrograph of Sample D indicated a particle size of about 20 nm, which is in good agreement with the crystallite size calculated from the XRD patterns. Table 2 shows the correlation between the properties of different samples generated through different synthetic procedures.

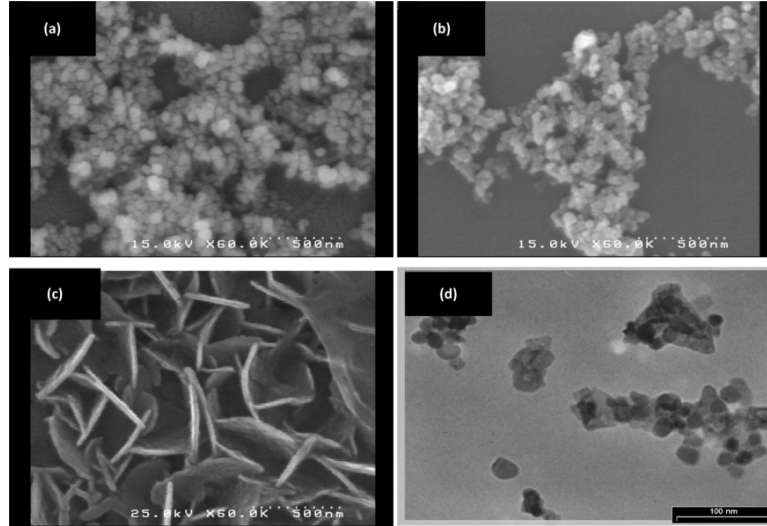


Figure 4: Planar micrographs of (a) SEM of Sample A, (b) SEM of Sample D, (c) SEM of Sample E, (d) TEM of Sample D.

Table 2: The correlation between different samples with different synthesis procedures and their properties.

Sample code	A	B	C	D	E
Morphology	spherical	spherical	spherical	spherical	flake
Crystallite size (nm)	16.6	17.5	16.1	18.9	16.5
Band gap (eV)	3.2	3.17	3.25	3.18	3.27

### 3.2 The Optical Properties of ZnO Nanoparticles

Absorption and fluorescence spectroscopies are powerful non-destructive techniques for exploring the optical properties of semiconducting nanoparticles. The absorption spectra of the samples are presented in Figure 5. All absorption curves exhibit an intense peak with an absorption edge in the range of 352–366 nm. The optical band gap ( $E_g$ ) was determined from the absorption spectra using the Tauc relationship as follows:

$$(\alpha h\nu) = A(h\nu - E_g)^n$$

where  $\alpha$  is the absorption coefficient,  $h$  is the Planck's constant,  $\nu$  is the photon frequency, and  $E_g$  is the optical band gap; the value of  $n$  is 0.5 for direct band gap semiconductors and 2 for indirect band gap semiconductors.<sup>23</sup> An extrapolation of the linear region of a plot of  $(\alpha h\nu)^2$  versus photon energy  $h\nu$  gives the value of the optical band gap (Figure 6). The derived optical band gap values for samples a-e were 3.2, 3.17, 3.25, 3.18 and 3.27 eV, respectively. The calculated optical band gap of the ZnO nanoparticles was found to decrease with increasing average crystallite size. The band gap values of Samples C and E were higher than the other samples due to smaller particle size. All of the  $E_g$  values were smaller than reported for bulk ZnO (3.37 eV). In the literature, the differences between the optical band gap and the band gap of bulk ZnO correlate to the presence of vacancies and dopants, which affect the electronic structures of nanoparticles.<sup>24</sup>

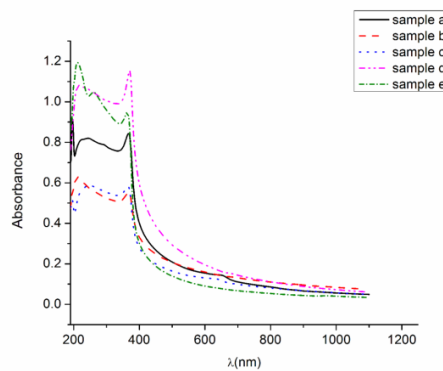


Figure 5: The UV-Vis absorption spectra for Samples A–E obtained by the mechanochemical method.

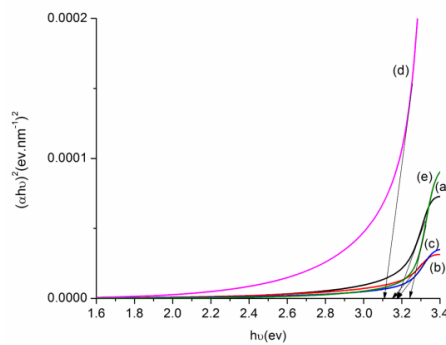


Figure 6: The Tauc plots for Samples A–E; the intersections of the tangent lines and the x-axis give the values of the optical band gaps for different samples.

PL spectroscopy can be used for the investigation of intrinsic defects in the ZnO nanoparticles. Figure 7 shows the PL spectra of different samples at room temperature. The UV emissions, observed 390 nm, were attributed to near-band-edge excitonic emission resulting from the recombination of electrons in the conduction band and holes in the valence band. A strong emission was also observed in the visible region at 620 nm. This emission was attributed to the red emission caused by defects such as zinc and oxygen anti-sites<sup>25</sup> and doubly charged oxygen vacancies.<sup>26</sup> The high impact energy of the ball-to-powder collisions may induce many crystallographic defects in powders treated by high-energy ball milling processes. During mechanical milling, vacancies in excess of the equilibrium level were produced by plastic deformation as a consequence of the movement and interaction of dislocations.<sup>27</sup> Based on the literature, smaller nanoparticles with higher surface area to volume ratios tend toward higher levels of surface oxygen vacancies.<sup>28</sup>

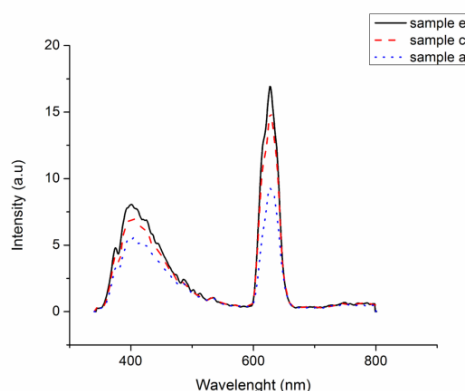


Figure 7: The photoluminescence spectra of Samples A, C and E at room temperature.

#### 4. CONCLUSIONS

ZnO nanoparticles of almost uniform size and morphology were synthesised using a simple, cost-effective one-step mechanochemical method. Spherical and flake-shape morphologies were obtained by changing the ordering of synthetic process. Increases in the milling energy led to slight increases in crystallite size (from ~16 to ~19 nm) as a result of cold welding. The optical band gap values for different ZnO nanoparticles were found to be smaller than known for bulk material. This result was consistent with PL studies and correlated to the existence of intrinsic defects in the synthesised nanoparticles.

## 5. ACKNOWLEDGEMENT

This work was financially supported by the Materials and Energy Research Center (MERC), Tehran, Iran.

## 6. REFERENCES

1. Rensmo, H. et al. (1997). High light-to-energy conversion efficiencies for solar cells based on nanostructured ZnO electrodes. *J. Phys. Chem. B*, 101(14), 2598–2601.
2. Huang, J. et al. (2011). Fabrication and gas-sensing properties of hierarchically porous ZnO architectures. *Sens. Actuators. B*, 155(1), 126–133.
3. Sirringhaus, H. (2005). Device physics of solution-processed organic field-effect transistors. *Adv. Mater.*, 17(20), 2411–2425.
4. Li, C. et al. (2010). Synthesis of ZnO/Zn<sub>2</sub>SiO<sub>4</sub>/SiO<sub>2</sub> composite pigments with enhanced reflectance and radiation-stability under low-energy proton irradiation. *Mater. Lett.*, 64(18), 1972–1974.
5. Akhavan, O. et al. (2009). Hydrothermal synthesis of ZnO nanorod arrays for photocatalytic inactivation of bacteria. *J. Phys. D: Appl. Phys.*, 42(22), 225–305.
6. Butt, F. K. et al. (2014). Synthesis of novel ZnV<sub>2</sub>O<sub>4</sub> hierarchical nanospheres and their applications as electrochemical supercapacitor and hydrogen storage material. *ACS Appl. Mater. Interfaces.*, 6(16), 13635–13641.
7. Butt, F. K. et al. (2014). Synthesis of novel ZnV<sub>2</sub>O<sub>4</sub> spinel oxide nanosheets and their hydrogen storage properties. *Cryst. Eng. Comm.*, 16(5), 894–899.
8. Butt, F. K. et al. (2014). Synthesis of mid-infrared SnSe nanowires and their optoelectronic properties. *Cryst. Eng. Comm.*, 16(17), 3470–3473.
9. Manzoor, U. et al. (2009). Quantum confinement effect in ZnO nanoparticles synthesized by co-precipitate method. *Physica E Low Dimens. Syst. Nanostruct.*, 41(9), 1669–1672.
10. Zak, A. K. et al. (2011). Effects of annealing temperature on some structural and optical properties of ZnO nanoparticles prepared by a modified sol–gel combustion method. *Ceram. Int.*, 37(1), 393–398.
11. Dai, Z. R., Pan, Z. W. & Wang, Z. L. (2003). Novel nanostructures of functional oxides synthesized by thermal evaporation. *Adv. Funct. Mater.*, 13(1), 9–24.
12. Damonte, L. C. et al. (2004). Nanoparticles of ZnO obtained by mechanical milling. *Powder Technol.*, 148(1), 15–19.

13. Lee, J. S. et al. (2003). ZnO nanomaterials synthesized from thermal evaporation of ball-milled ZnO powders. *J. Crystal Growth.*, 254, 423–431.
14. Radoi, R. et al. (2003). Luminescence properties of mechanically milled and laser irradiated ZnO. *Nanotechnol.*, 14(7), 794.
15. Ao, W. et al. (2006). Mechanochemical synthesis of zinc oxide nanocrystalline. *Powder Technol.*, 168(3), 148–151.
16. Koch, C. (1997). Synthesis of nanostructured materials by mechanical milling: problems and opportunities. *Nanostruct. Mater.*, 9(1–8), 13–22.
17. Tsuzuki, T. & McCormick, P. G. (2004). Mechanochemical synthesis of nanoparticles. *J. Mater. Sci.*, 39(16), 5143–5146.
18. Tsuzuki, T. & McCormick, P. G. (2001). ZnO nanoparticles synthesised by mechanochemical processing. *Scripta Mater.*, 44(8–9), 1731–1734.
19. Dodd, A. et al. (2008). A comparative evaluation of the photocatalytic and optical properties of nanoparticulate ZnO synthesised by mechanochemical processing. *J. Nanopart. Res.*, 10(1), 243–248.
20. Moballegh, A. et al. (2007). ZnO nanoparticles obtained by mechanochemical technique and the optical properties. *Surf. Sci.*, 601(13), 2850–2854.
21. Dhara, S. & Giri, P. (2011). Quick single-step mechanosynthesis of ZnO nanorods and their optical characterization: Milling time dependence. *Appl. Nanosci.*, 1(4), 165–171.
22. Lu, J., Ng, K. M. & Yang, S. (2008). Efficient, one-step mechanochemical process for the synthesis of ZnO nanoparticles. *Ind. Eng. Chem. Res.*, 47(4), 1095–1101.
23. Makkar, M. & Bhatti, H. (2011). Inquisition of reaction parameters on the growth and optical properties of ZnO nanoparticles synthesized via low temperature reaction route. *Chem. Phys. Lett.*, 507(1–3), 122–127.
24. Zandi, S. et al. (2011). Microstructure and optical properties of ZnO nanoparticles prepared by a simple method. *Phys. B: Condensed Mater.*, 406(17), 3215–3218.
25. Singh, A., Viswanath, V. & Janu, V. (2009). Synthesis, effect of capping agents, structural, optical and photoluminescence properties of ZnO nanoparticles. *J. Lumin.*, 129(8), 874–878.
26. Fan, Z. et al. (2004). Photoluminescence and polarized photodetection of single ZnO nanowires. *Appl. Phys. Lett.*, 85(25), 6128–6130.
27. Zhang, B., Lu, L. & Lai, M. (2003). Evolution of vacancy densities in powder particles during mechanical milling. *Phys. B: Condensed Mater.*, 325, 120–129.
28. Huang, M. H. et al. (2001). Catalytic growth of zinc oxide nanowires by vapour transport. *Adv. Mater.*, 13(2), 113–116.